Hydrodynamic torques from symmetry

B. Mehlig

Department of Physics,

University of Gothenburg, Sweden

Workshop *Chiral particles and odd fluids*, Eindhoven January 12-14 (2026)

Outline

Transport of microplastic particles in the atmosphere depends on particle shape.

Tatsii, Bucci, Bhowmick, Güttler, Bakels, Bagheri & Stohl, Environ. Science & Tech. (2024)

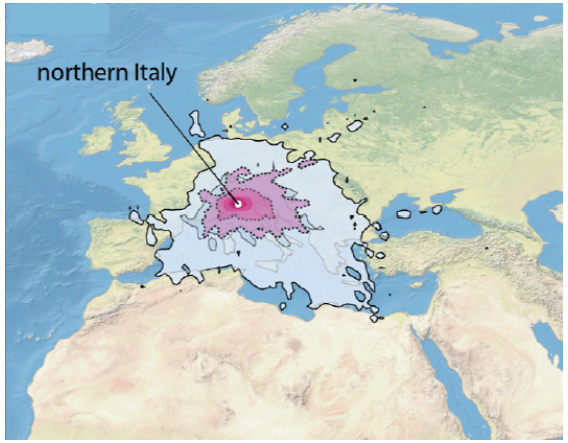

Goals

—understand how particle shape affects particle translation and rotation,

—parameterise force and torque on particles of arbitrary shape.

Challenges

—Asymmetric shapes require new force and torque parameterisations.

—Large settling speed v_g ⇨ *fluid inertia* matters (particle Reynolds number $\mathrm{Re}_p = a v_g/\nu$).

—Mass-density ratio $\mathscr{R} = \varrho_p/\varrho_f \sim 1000$ ⇨ *particle inertia* matters (Stokes number St).

Stokes limit

Settling in quiescent fluid

How does particle shape affect the path of a small particle settling in a quiescent fluid?

Stokes flow. Hydrodynamic force $\boldsymbol{F}$ and torque $\boldsymbol{T}$ in a quiescent fluid:

$$\begin{bmatrix} \boldsymbol{F} \\ \boldsymbol{T} \end{bmatrix} = -\mu \begin{bmatrix} \mathbb{A} & \mathbb{B}^{\mathsf{T}} \\ \mathbb{B} & \mathbb{C} \end{bmatrix} \begin{bmatrix} \boldsymbol{v} \\ \boldsymbol{\omega} \end{bmatrix} .$$

particle velocity $\boldsymbol{v}$
angular velocity $\boldsymbol{\omega}$

Resistance tensors $\mathbb{A}$, $\mathbb{B}$, $\mathbb{C}$. Viscosity μ.

For non-zero translation-rotation coupling $\mathbb{B}$, intricate settling dynamics (rotation, translation) in quiescent fluid.

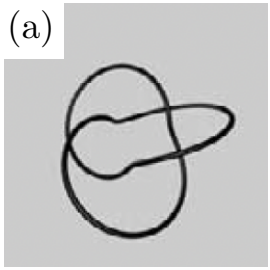

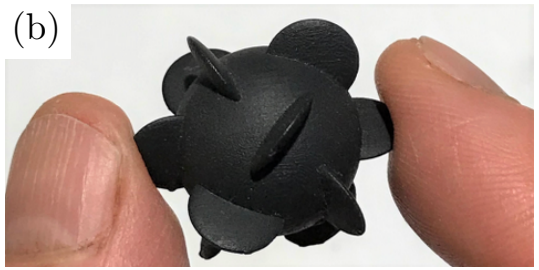

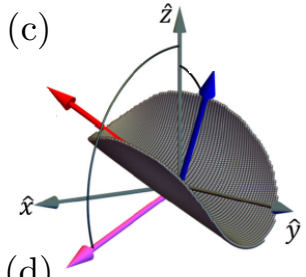

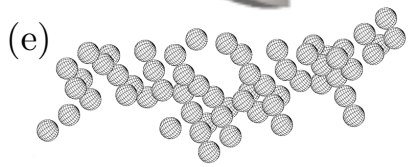

(a) Gonzalez, Graf & Maddocks, JFM (2004)
(b) Collins, Hamati, Candelier, Gustavsson, Mehlig & Voth, PRF (2021)
(c) Miara, Vaquero-Stainer, Pihler-Puzovic, Heil & Juel, Communications Physics (2024)
(d) Huseby, Gissinger, Candelier, Pujara, Verhille, Mehlig & Voth, Phys. Rev. Fluids (2025)
(e) Gissinger, Huseby, Candelier, Gustavsson, Voth & Mehlig (2026)

Isotropic helicoid

Collins, Hamati, Candelier, Gustavsson, Mehlig & Voth, Phys. Rev. Fluids (2021)

Lord Kelvin's isotropic helicoid (inviscid limit)

> '*An isotropic helicoid may be made by attaching projecting vanes to the surface of a globe in proper positions [...]. By making the globe and the vanes of light paper, a body is obtained rigid enough and light enough to illustrate by its motions through air the motions of an isotropic helicoid through an incompressible liquid*' Lord Kelvin, "Hydrokinetic solutions and observations," Phil. Mag. **42**, 362 (1871).

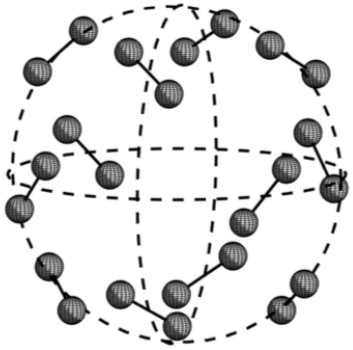

Drag independent of particle orientation ($\mathbb{A} = a\mathbb{I}$) like a sphere, but translation-rotation coupling $\mathbb{B} \neq 0$, like a propeller.

Experiments appear to indicate $\mathbb{B} = 0$.

Perturbation theory for isotropic helicoidal aggregate made out of non-chiral vanes with resistance tensors $\mathbb{A}_m^{(\mathrm{v})} = [\mathbb{A}_m^{(\mathrm{v})}]^{\mathsf{T}}$ gives $\mathbb{B} = \underbrace{\sum_m \boldsymbol{r}_m \wedge \mathbb{A}_m^{(\mathrm{v})}}_{=0} + \underbrace{\sum_m \boldsymbol{r}_m \wedge \delta\mathbb{A}_m^{(\mathrm{v})}}_{\neq 0}$
(vectors $\boldsymbol{r}_m$ from c.o.m. to centre of vane m).

since $\mathbb{A}_m^{(\mathrm{v})} = [\mathbb{A}_m^{(\mathrm{v})}]^{\mathsf{T}}$ non-interacting

since $\delta\mathbb{A}_m^{(\mathrm{v})} \neq [\delta\mathbb{A}_m^{(\mathrm{v})}]^{\mathsf{T}}$ first-order hydrodynamic interactions between vanes

⇨ time-reversal symmetry ($\mathbb{A}_m^{(\mathrm{v})} = [\mathbb{A}_m^{(\mathrm{v})}]^{\mathsf{T}}$) causes weak but non-zero coupling.

Shear flow

Fries, Kumar, Mihiretie, Hanstorp & Mehlig, Phys. Fluids **30** (2018) 033304

Angular dynamics in shear flow $\boldsymbol{U} = \mathbb{A} \cdot \boldsymbol{x}$:

$$\begin{bmatrix} \boldsymbol{F} \\ \boldsymbol{T} \end{bmatrix} = \mu \begin{bmatrix} \mathbb{A} & \mathbb{B}^{\mathsf{T}} & \widetilde{\mathbb{G}} \\ \mathbb{B} & \mathbb{C} & \widetilde{\mathbb{H}} \end{bmatrix} \begin{bmatrix} \boldsymbol{U} - \boldsymbol{v} \\ \boldsymbol{\Omega} - \boldsymbol{\omega} \\ \mathbb{S} \end{bmatrix}$$

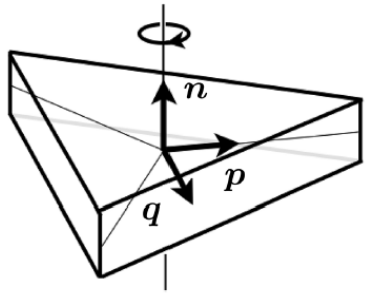

Vorticity $\boldsymbol{\Omega}$ ($\Omega_i = -\frac{1}{2}\epsilon_{ijk}O_{jk}$), $\mathbb{O}$ and $\mathbb{S}$ are anti-symmetric and symmetric parts of $\mathbb{A}$.

Overdamped approximation ($\boldsymbol{T} = 0$) and no slip ($\boldsymbol{v} = \boldsymbol{U}$) yields $\boldsymbol{\omega} = \boldsymbol{\Omega} + \mathbb{C}^{-1}\widetilde{\mathbb{H}} : \mathbb{S}$ in the usual way.

Prismatic symmetry D_{3h}: $\boldsymbol{\omega} = \boldsymbol{\Omega} - \Lambda(\mathbb{S}\boldsymbol{n}) \wedge \boldsymbol{n}$, and thus

$$\dot{\boldsymbol{n}} = \mathbb{O}\boldsymbol{n} + \Lambda[\mathbb{S}\boldsymbol{n} - (\boldsymbol{n} \cdot \mathbb{S}\boldsymbol{n})\,\boldsymbol{n}]$$

Shape parameter Λ .
Known for ellipsoids and cuboids.
Jeffery, Proc. Roy. Soc. London Ser. A **102** (1922) 161
Bretherton, JFM **14** (1964) 284

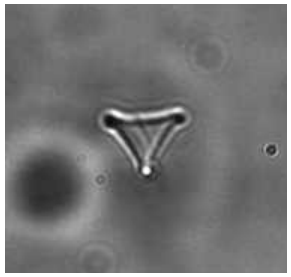

micron-sized platelet in micro-channel flow

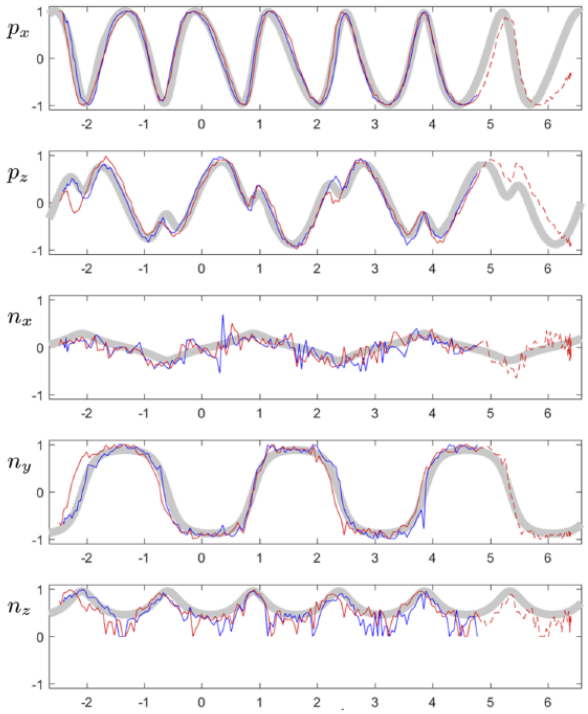

c.o.m. displacement

Broken reflection symmetries

Fries, Einarsson & Mehlig, Phys. Rev. Fluids **2** (2017) 014302

Angular dynamics in shear flow $\boldsymbol{U} = \mathbb{A} \cdot \boldsymbol{x}$:

$$\begin{bmatrix} \boldsymbol{F} \\ \boldsymbol{T} \end{bmatrix} = \mu \begin{bmatrix} \mathbb{A} & \mathbb{B}^{\mathsf{T}} & \widetilde{\mathbb{G}} \\ \mathbb{B} & \mathbb{C} & \widetilde{\mathbb{H}} \end{bmatrix} \begin{bmatrix} \boldsymbol{U} - \boldsymbol{v} \\ \boldsymbol{\Omega} - \boldsymbol{\omega} \\ \mathbb{S} \end{bmatrix}$$

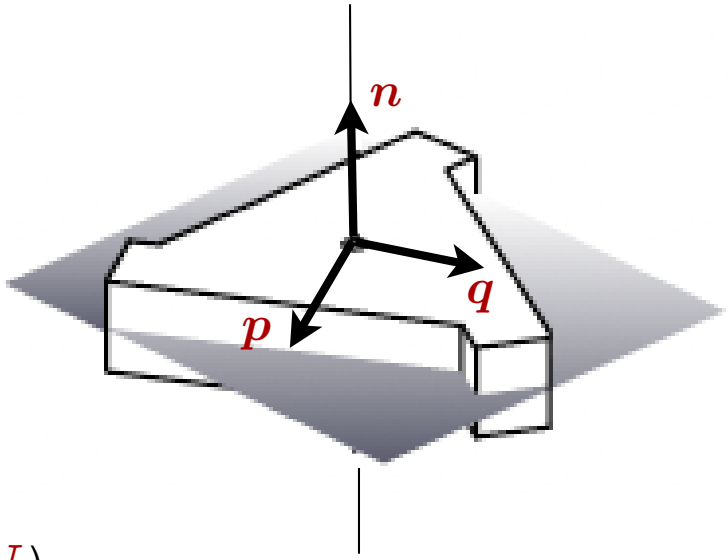

Vorticity $\boldsymbol{\Omega}$ ($\Omega_i = -\frac{1}{2}\epsilon_{ijk}O_{jk}$), $\mathbb{O}$ and $\mathbb{S}$ are anti-symmetric and symmetric parts of $\mathbb{A}$.

.

Overdamped approximation ($\boldsymbol{T} = 0$) and no slip ($\boldsymbol{v} = \boldsymbol{U}$) yields $\boldsymbol{\omega} = \boldsymbol{\Omega} + \mathbb{C}^{-1}\widetilde{\mathbb{H}} : \mathbb{S}$ in the usual way.

Particle with three-fold rotation symmetry around $\boldsymbol{n}$, and only one reflection symmetry in orthogonal plane. Symmetry analysis: $\boldsymbol{\omega} = \boldsymbol{\Omega} - \Lambda(\mathbb{S}\boldsymbol{n}) \wedge \boldsymbol{n} + \Gamma(\boldsymbol{n} \cdot \mathbb{S}\boldsymbol{n})\boldsymbol{n} + \Psi\mathbb{S}\boldsymbol{n}$, and thus

$$\dot{\boldsymbol{n}} = \mathbb{O}\boldsymbol{n} + \Lambda[\mathbb{S}\boldsymbol{n} - (\boldsymbol{n} \cdot \mathbb{S}\boldsymbol{n})\,\boldsymbol{n}] + \Psi(\mathbb{S}\boldsymbol{n}) \wedge \boldsymbol{n}$$
$$\boldsymbol{\omega} \cdot \boldsymbol{n} = \boldsymbol{\Omega} \cdot \boldsymbol{n} + (\Gamma + \Psi)\boldsymbol{n} \cdot \mathbb{S}\boldsymbol{n}$$

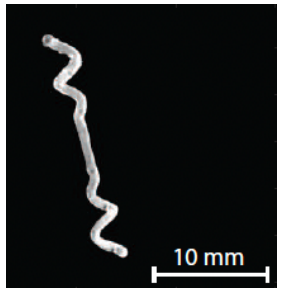

For $\Gamma = \Psi = 0$, Jeffery dynamics with Bretherton parameter Λ , but not otherwise. For $\Psi = 0$, same dynamics as *chiral dipole*.

Kramel, Voth, Tympel & Toschi, Phys. Rev. Lett. **117** (2016)

Summary — particle-shape symmetries

Transform $\boldsymbol{F}(\boldsymbol{v},\boldsymbol{\omega})$ and $\boldsymbol{T}(\boldsymbol{v},\boldsymbol{\omega})$ by orthogonal transformation $\mathbb{R}$ as

Bretherton, J. Fluid Mech. **14** (1962) 284
Happel & Brenner, *Low Reynolds Number Hydrodynamics* (1983)
Fries, Einarsson, and Mehlig, Phys. Rev. Fluids **2** (2017) 014302
Witten & Diamant, Rep. Prog. Phys. **83**, (2020) 116601

$$\boldsymbol{F}' = \boldsymbol{F}(\mathbb{R}\boldsymbol{v}, \det[R]\mathbb{R}\boldsymbol{\omega}) \quad \text{and} \quad \boldsymbol{T}' = \boldsymbol{T}(\mathbb{R}\boldsymbol{v}, \det[\mathbb{R}]\mathbb{R}\boldsymbol{\omega})\,.$$

If the particle shape remains invariant under $\mathbb{R}$, then $\boldsymbol{F}' = \mathbb{R}\boldsymbol{F}$ and $\boldsymbol{T}' = \det[\mathbb{R}]\mathbb{R}\boldsymbol{T}$. Using

$$\begin{bmatrix}\boldsymbol{F}\\ \boldsymbol{T}\end{bmatrix} = -\mu \begin{bmatrix}\mathbb{A} & \mathbb{B}^{\mathsf{T}}\\ \mathbb{B} & \mathbb{C}\end{bmatrix}\begin{bmatrix}\boldsymbol{v}\\ \boldsymbol{\omega}\end{bmatrix},$$

one concludes that the elements of the resistance tensors are constrained by:

$$\begin{aligned} A_{ij} &= R_{mi}A_{mn}R_{nj}\,,\\ B_{ij} &= \det[\mathbb{R}]R_{mi}B_{mn}R_{nj}\,,\\ C_{ij} &= R_{mi}C_{mn}R_{nj}\,. \end{aligned}$$

Einstein summation convention
(repeated indices are summed over)

⇨ point-group symmetries of particle shape constrain certain elements A_{ij} , B_{ij} , C_{ij} to vanish. Similarly

$$\widetilde{G}_{ijk} = R_{mi}\widetilde{G}_{mnl}R_{nj}R_{lk} \quad \text{and} \quad \widetilde{F}_{ijk} = \det[\mathbb{R}]\, R_{mi}\widetilde{F}_{mnl}R_{nj}R_{lk}$$

Beyond Stokes limit: fluid inertia

Alignment of atmospheric ice crystals

Reflection of polarised light shows that small ice platelets align in mixed-phase clouds.

Breon & Dubrulle, J. Atmos Sci. **61** (2004) 2888

Fluid acceleration results in *fluid-inertia* torque that aligns particles in quiescent fluid.

At large settling speeds, fluid-inertia torque dominates

⇨ rods align with $\boldsymbol{n} \perp \hat{\boldsymbol{g}}$, disks with $\boldsymbol{n} \parallel \hat{\boldsymbol{g}}$.

Cox, J. Fluid Mech. **23** (1965) 625

Khayat & Cox, J. Fluid Mech. **209** (1989) 435

Klett, J. Atmos. Sci. **52** (1995) 2276

Turbulent fluid-velocity gradients disrupt alignment.

Variance of tilt angle θ (angle between $\boldsymbol{n}$ and $\hat{\boldsymbol{g}}$)?

Kramel, PhD thesis, Wesleyan University (2017)

Lopez & Guazzelli, Phys. Rev. Fluids **2** (2017)

Gustavsson, Sheikh, Lopez, Naso, Pumir & Mehlig, NJP **21** (2019)

Roy, Kramel, Menon, Voth & Koch, J. Nonnewton. Fluid Mech. **318** (2023)

Most experiments and theory in water (overdamped).

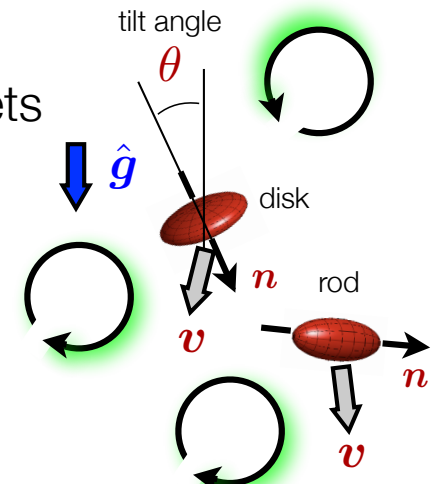

F. Waitz (KIT)

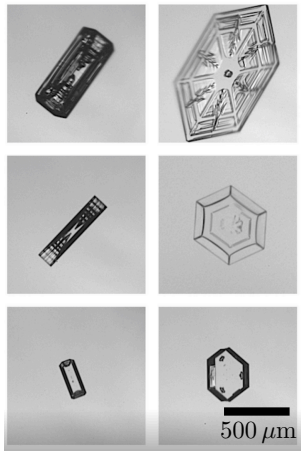

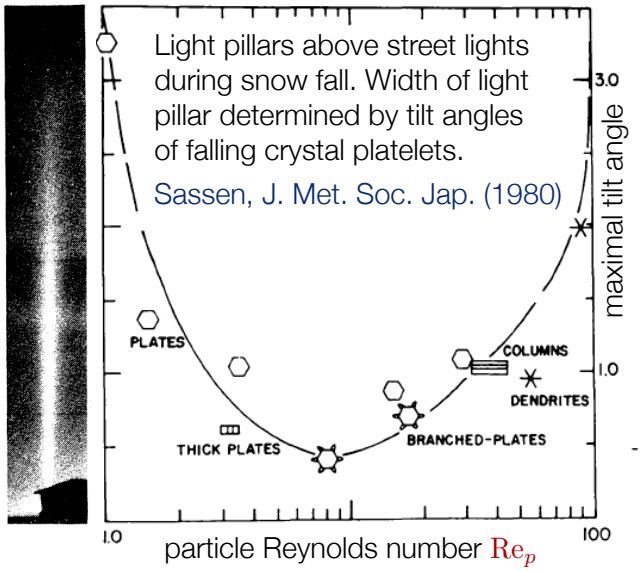

Lab experiments for spheroids in air

Gustavsson, Sheikh, Naso, Pumir & Mehlig, J. Atmos. Sci. **78** (2021)
Bhowmick, Seesing, Gustavsson, Güttler, Wang, Pumir, Mehlig & Bagheri, PRL (2024)

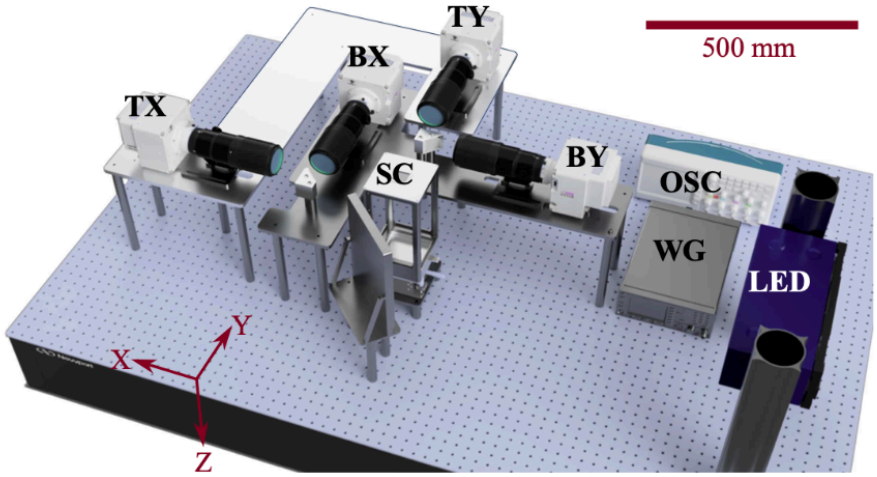

Group	λ	$2a_{\parallel}$ [μm]	$2a_{\perp}$ [μm]	V_p [mm^3]	Re_p	τ_p [ms]
I	0.20	47.9	239.4	1.44×10^{-3}	2.8	42.0
I	0.50	88.2	176.4	1.44×10^{-3}	2.5	57.0
I	0.80	120.6	150.8	1.44×10^{-3}	2.4	66.7
I	1.00	140.0	140.0	1.44×10^{-3}	2.2	71.8
I	1.25	162.0	130.0	1.44×10^{-3}	2.6	77.2
I	2.00	222.2	111.0	1.44×10^{-3}	3.3	90.4
I	5.00	410.0	81.8	1.44×10^{-3}	5.0	122.9
II	0.25	65.5	261.9	2.35×10^{-3}	3.8	62.9
II	4.00	399.4	99.9	2.08×10^{-3}	5.9	146.3
III	0.25	150.0	600.0	28.28×10^{-3}	22.5	329.9
III	4.00	876.9	219.2	22.07×10^{-3}	34.3	704.6

μm-sized spheroids settling in still air

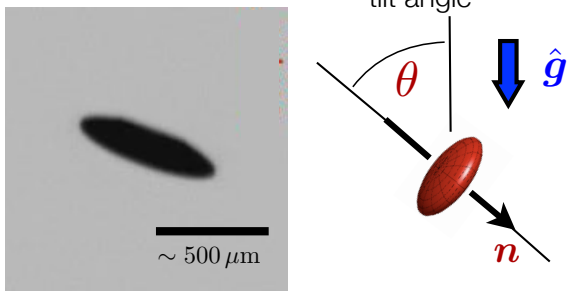

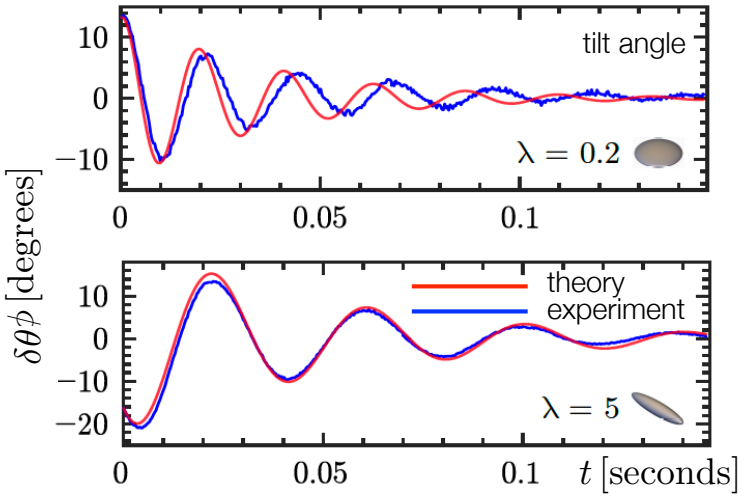

Oscillations due to particle inertia.
Harmonic-oscillator model for θ (——).

Asymmetric particles

Volcanic ash Bagheri & Bonaddona, Powder Technol. (2016)
Cloud-ice crystals Kajikawa, J. Meteor. Soc. Japan (1972)
Microplastics Allen *et al.* Nature Geoscience (2019)

(a) Candelier & Mehlig, J. Fluid Mech. (2016)
(b) Roy, Hamati, Tierney, Koch & Voth, J. Fluid Mech. (2019)
(c) Pruppacher & Klett (1997)
(d) Cai *et al.,* J. Cleaner Prod. (2020)
(e) Candelier, Gustavsson, Sharma, Sundberg, Pumir, Bagheri & Mehlig, Phys. Rev. Res. (2025)
(f) Maches, Houssais, Sauret & Meiburg, J. Fluid Mech. (2024)
(g) Flapper, Piumini, Verzicco, Huismann & Lohse (2026)

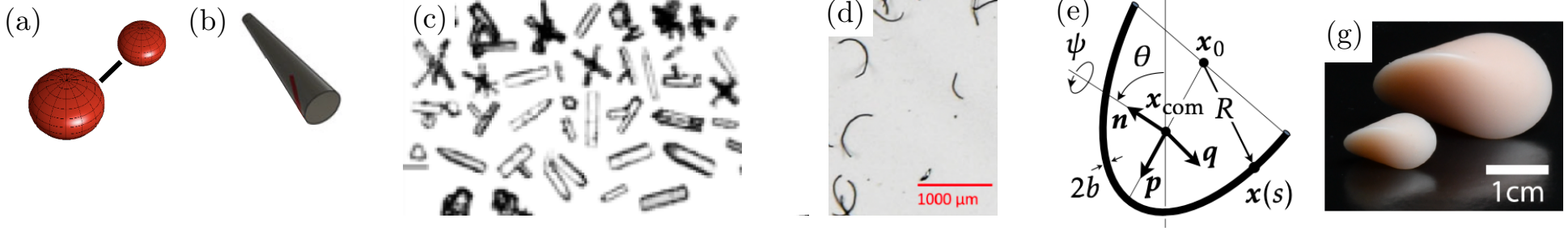

Broken fore-aft symmetry

Candelier & Mehlig, J. Fluid Mech. **802** (2016) 174

How does breaking of fore-aft symmetry change angular dynamics?

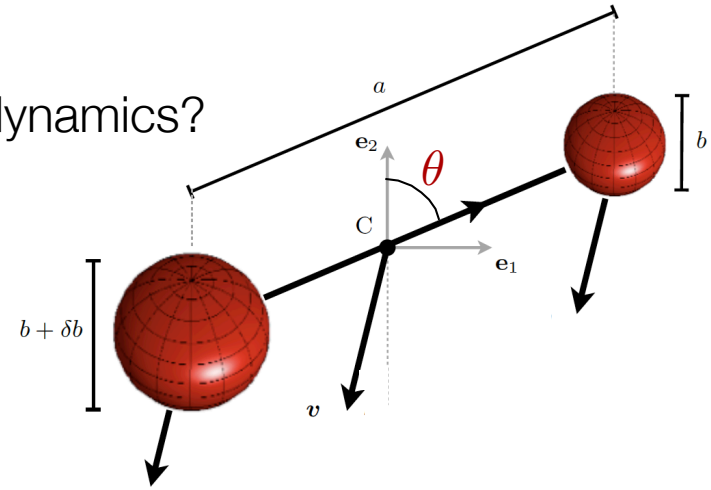

Asymmetric dumbbell at $\mathrm{Re_p} \approx 0$ turns so that larger sphere settles first (spheres have same mass density).

Asymmetric dumbbell to first order in $\mathrm{Re_p}$: hydrodynamic and inertial torques balance at angle θ that depends on asymmetry $\delta b/b$ and $\mathrm{Re_p}$.

Prediction: asymmetric rods settle at a steady angle θ different from $\frac{\pi}{2}$.

Roy, Hamati, Tierney, Koch & Voth, JFM (2019)

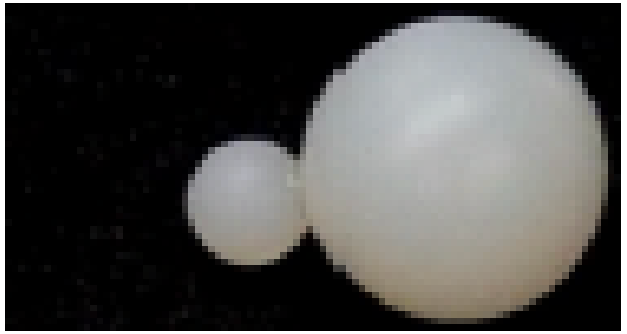

Maches, Houssais, Sauret & Meiburg, JFM (2024)

Curved atmospheric fibres

Candelier, Gustavsson, Sharma, Sundberg, Pumir, Bagheri & Mehlig, Phys. Rev. Fluids (2025)

Tatsii *et al.*, Environ. Science & Tech. (2024)

Stokes limit: curved fibres settle like this:

Fluid inertia: circles settle like this:

How does shape (aspect ratio, size, radius of curvature) determine settling angle of curved fibre?

Non-dimensional parameters:
Mass-density ratio $\mathscr{R} = \rho_p/\rho_f$
Non-dimensional particle volume $\mathscr{V} = 2\pi a b^2 g/\nu^2$
Aspect ratio $\kappa = a/b$ (contour length $2a$)
Radius of curvature $R/a = M/\pi \quad (M = 2, 4, \ldots)$
Inertia parameter $\mathscr{R}\mathscr{V}$

(related to Galileo number Fornari, Picano, Sardina & Brandt, JFM (2016) and particle Reynolds number.
Inertia parameter $I^* \sim \lambda\mathscr{R}$ for disks Auguste, Magnaudet & Fabre, JFM (2013))

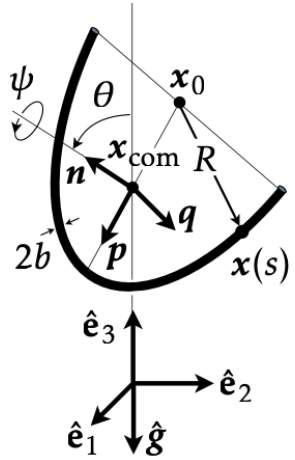

Inertial torques on curved fibres

Candelier, Gustavsson, Sharma, Sundberg, Pumir, Bagheri & Mehlig, Phys. Rev. Fluids (2025)

We computed inertial forces and torques on curved planar fibre settling in quiescent fluid using *slender-body theory*.

Khayat & Cox, JFM **209** (1989) 435

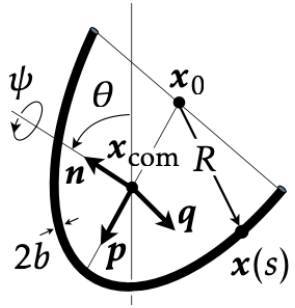

Inertial torque (settling speed $\boldsymbol{v} = v\hat{\boldsymbol{v}}$, contour length $2a$) in the particle-fixed frame to order Re_p

$$T_p^{(1)}/(2\pi\mu v a^2) = \frac{av}{\nu(\log\kappa)^2} c_{pqn}\hat{v}_q\hat{v}_n\,,$$

$$T_q^{(1)}/(2\pi\mu v a^2) = \frac{av}{\nu(\log\kappa)^2} c_{qpn}\hat{v}_p\hat{v}_n\,,$$

$$T_n^{(1)}/(2\pi\mu v a^2) = \frac{av}{\nu(\log\kappa)^2} \left[c_{npq}\hat{v}_p\hat{v}_q + b_{nq}\hat{v}_q + d_{nqnn}\hat{v}_q\hat{v}_n^2 + d_{nqqq}\hat{v}_q^3\right]$$

geometrical coefficients $b_{nq}, c_{pqn}, \ldots$ (fibre curvature)
viscosity $\mu = \rho_f \nu$

Different from Khayat-Cox torque for straight fibre.

Need to consider all three components of the torque.

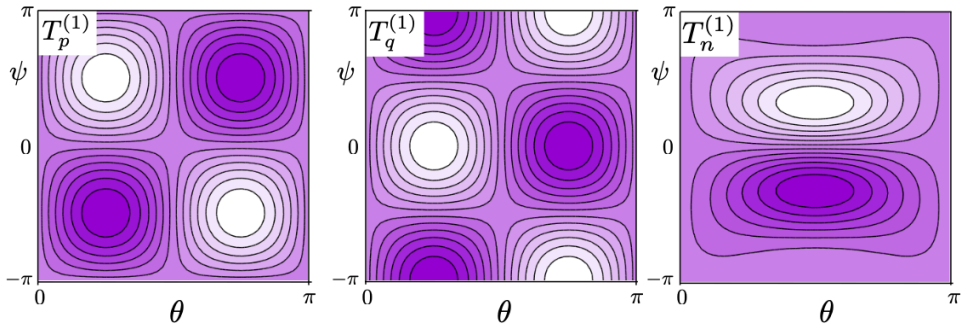

Comparison model & experiment

Candelier, Gustavsson, Sharma, Sundberg, Pumir, Bagheri & Mehlig, Phys. Rev. Fluids (2025)

Compare full slender-body theory (not only terms linear in Re_p) with experiment.

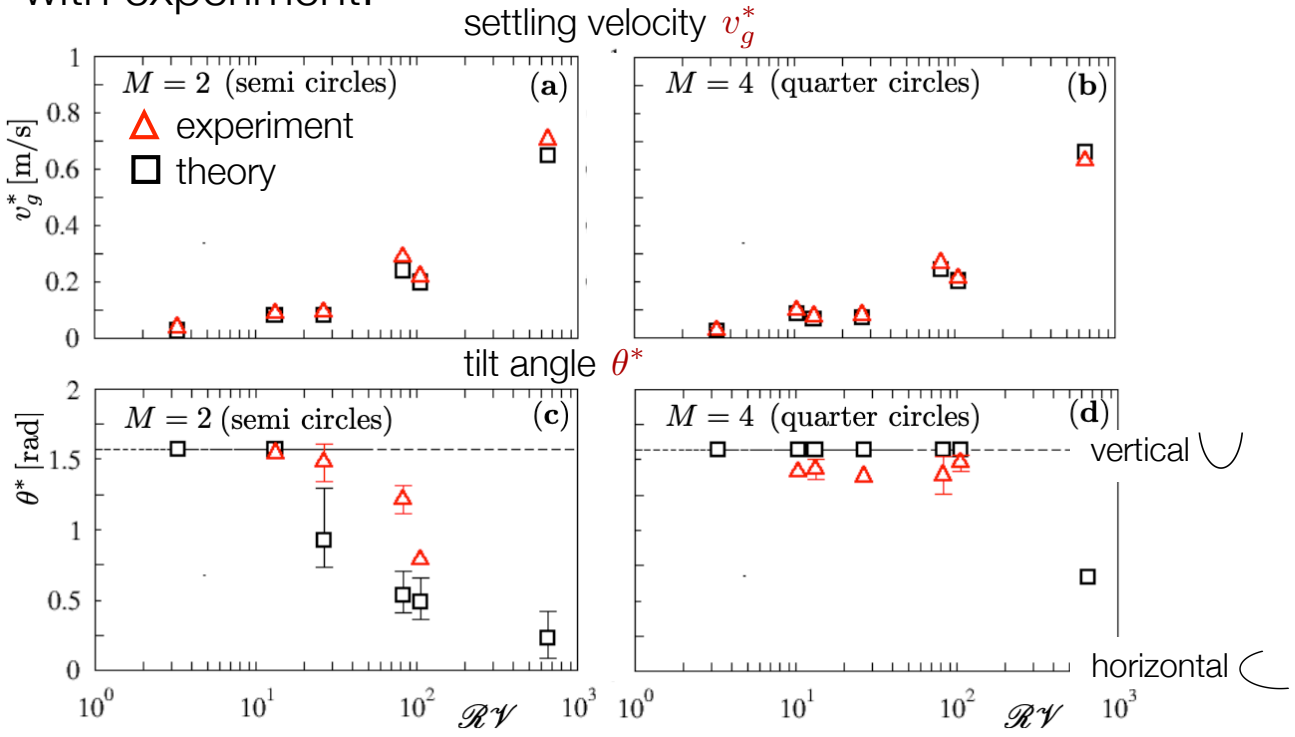

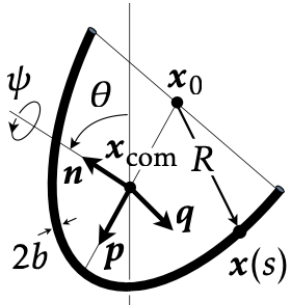

κ	$2a$	$2b$	$\langle v_g \rangle$	Re_a	$\mathscr{RV}$	ψ^*	θ^*	N
			semi-circular fibres					
20	2	0.1	0.704	47	660	–[a]	–[a]	9
	1	0.05	0.288	9.6	83	0.013±0.024	1.21±0.1	8
50	2	0.04	0.218	14.5	110	0	0.79	1
	1	0.02	0.086	2.9	13	0	1.54	1
100	2	0.02	0.094	6.2	26	0	1.48±0.13	5
	1	0.01	0.037	1.24	3.3	*[b]	*[b]	0
			quarter-circular fibres					
20	2	0.1	0.631	42	660	–[a]	–[a]	8
	1	0.05	0.265	8.8	83	-0.03±0.01	1.34±0.13	10
	0.5	0.025	0.096	1.6	10	-0.017	1.414	1
50	2	0.04	0.209	14.0	110	-0.003±0.017	1.48±0.06	11
	1	0.02	0.074	2.5	13	0	1.43±0.07	2
100	2	0.02	0.080	5.3	26	0	1.379	1
	1	0.01	0.026	0.88	3.3	*[b]	*[b]	0

[a] '–' no steady state observed.
[b] '*' fibre images blurred, orientations could not be determined.

Non-dimensional parameters $\mathscr{R} = \rho_p/\rho_f$ and $\mathscr{V} = 2\pi a b^2 g/\nu^2$, radius of curvature $R/a = M/\pi$, aspect ratio $\kappa = a/b$.

Comparison model & experiment

Candelier, Gustavsson, Sharma, Sundberg, Pumir, Bagheri & Mehlig, Phys. Rev. Fluids (2025)

Planar curved fibres settle at a steady tilt angle θ^* with gravity.

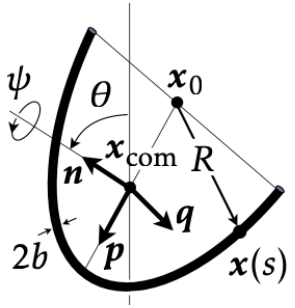

Depends sensitively on radius of curvature $R/a = M/\pi$ and inertia $\mathscr{RV}$.

Good overall agreement with experiment for not too large $\mathscr{RV}$, except in transition region

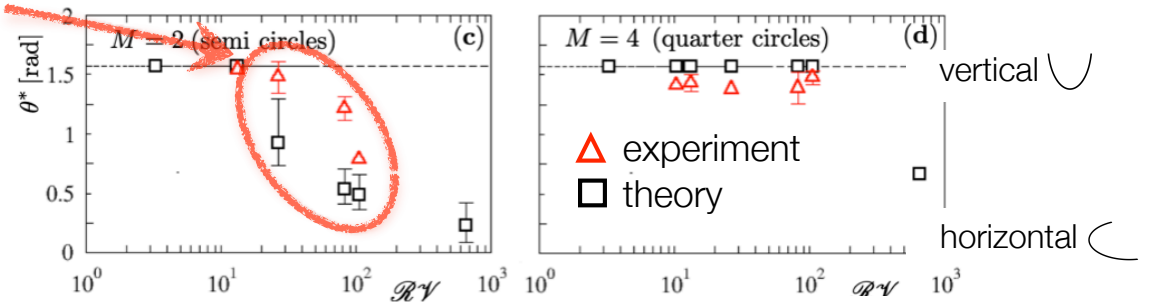

Large $\mathscr{RV}$: no alignment, unsteady dynamics.

Sequence of bifurcations to chaotic transient not understood.

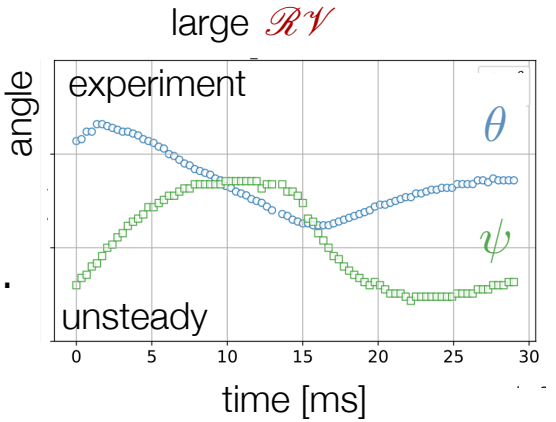

Symmetry analysis

Asymptotic matching

Sundberg, Candelier, Fintzi, Voth, Pierson, Gustavsson & Mehlig (2025)

Kernels $\mathbb{K}^{(1)}$, $\mathbb{K}^{(2)}$ analogous to (but different from) BBO history kernels, and $\boldsymbol{f}^{(0)} = \mathbb{A}\boldsymbol{v} + \mathbb{B}^{\mathsf{T}}\boldsymbol{\omega}$.

At non-zero but small Re_p

$$\boldsymbol{T} = \boldsymbol{T}^{(0)} + \mathrm{Re}_p \boldsymbol{T}^{(1)}_{\mathrm{reg}} + \sqrt{\mathrm{Re}_p \mathrm{Sl}}\, \boldsymbol{T}^{(1)}_{\mathrm{sing}} + \ldots$$

$$\boldsymbol{T}^{(1)}_{\mathrm{reg}} = \mathbb{N}^{(vv)} : \boldsymbol{v}\otimes\boldsymbol{v} + \mathbb{N}^{(\omega\omega)} : \boldsymbol{\omega}\otimes\boldsymbol{\omega} + \mathbb{N}^{(v\omega)} : \boldsymbol{v}\otimes\boldsymbol{\omega}\,.$$

$$\boldsymbol{T}^{(1)}_{\mathrm{sing}} = \mathbb{B}\cdot\int_0^t \mathrm{d}\tau\; \mathbb{K}^{(1)}(t,\tau)\cdot\frac{\mathrm{d}\boldsymbol{f}^{(0)}(\tau)}{\mathrm{d}\tau} + \sqrt{\mathrm{Re}_p/\mathrm{Sl}}\int_0^t \mathrm{d}\tau\; \mathbb{K}^{(2)}(t,\tau)\cdot\boldsymbol{f}^{(0)}(\tau)$$

$$\approx -\frac{3v}{32\pi}\sqrt{\frac{\mathrm{Re}_p}{\mathrm{Sl}}}\;\mathbb{B}\big[\mathbb{A}\boldsymbol{v} - \tfrac{1}{3}(\hat{\boldsymbol{v}}\otimes\hat{\boldsymbol{v}})\mathbb{A}\boldsymbol{v}\big]$$

Cox, J. Fluid Mech. 23 (1965) 625–643

in steady limit $1 \gg \mathrm{Re}_p \gg \mathrm{Re}_p\mathrm{Sl}$ (Strouhal number Sl measures unsteadiness).

Particle-shape symmetries constrain $\mathbb{A}$, $\mathbb{B}$, and $\mathbb{N}$-coefficients (just like $\widetilde{\mathbb{F}}$)

$$N^{(vv)}_{ijk} = \det[\mathbb{R}]\, R_{mi} N^{(vv)}_{mnl} R_{nj} R_{lk}\ .$$

Point-group symmetries of particle shapes

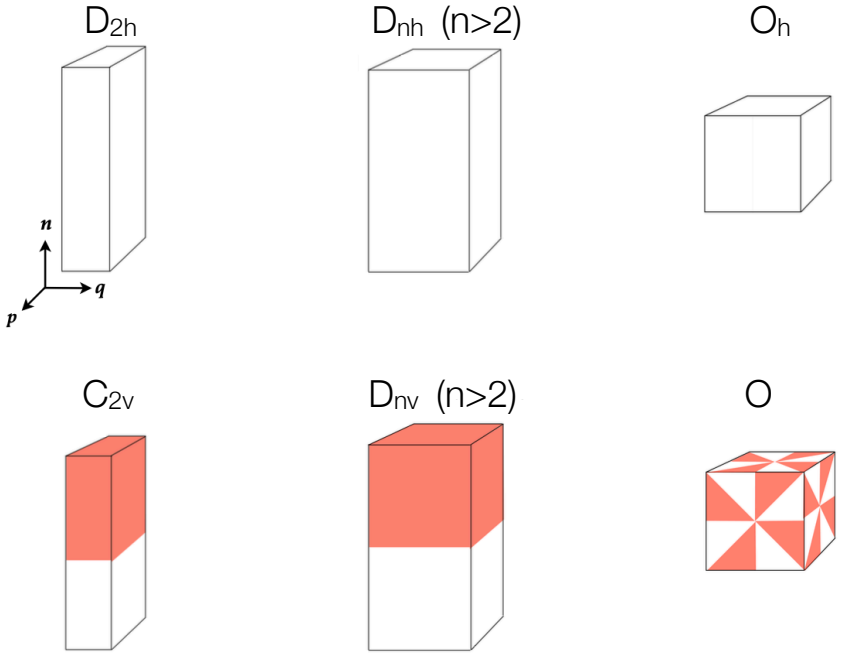

Fore-aft symmetry breaking

Sundberg, Candelier, Fintzi, Voth. Pierson, Gustavsson & Mehlig (2025)

Point-group symmetry C_{nv} with $n > 2$. In the particle-fixed basis

$$\boldsymbol{T}^{(1)} = g(v, v_n)(\hat{\boldsymbol{v}} \wedge \hat{\boldsymbol{n}})$$

$$g(v, v_n) = -v^2 B[2A_\perp + (A_\perp - A_\parallel)v_n^2]/(32\pi) + v^2(N_1^{(vv)} + N_2^{(vv)})v_n$$

with coefficients $A_\perp$, $A_\parallel$, B (translation-rotation coupling), and $N_1^{(vv)} + N_2^{(vv)}$.

This explains results of experiments, direct numerical simulations, and model calculations.

(a) Candelier & Mehlig, JFM (2016)
(b) Roy, Hamati, Tierney, Koch & Voth, JFM (2019)
(c) Maches, Houssais, Sauret & Meiburg, JFM (2024)

Ellipsoid

Bhowmick, Wang, Latt & Bagheri, JFM **1021** (2025)

Lab experiments and particle-resolved simulations of ellipsoidal particles settling in quiescent air show:

— ellipsoid aligns with broadest sign down
— intricate dependence of transient on shape

To understand this, require all three components of fluid-inertia torque. From symmetry analysis:

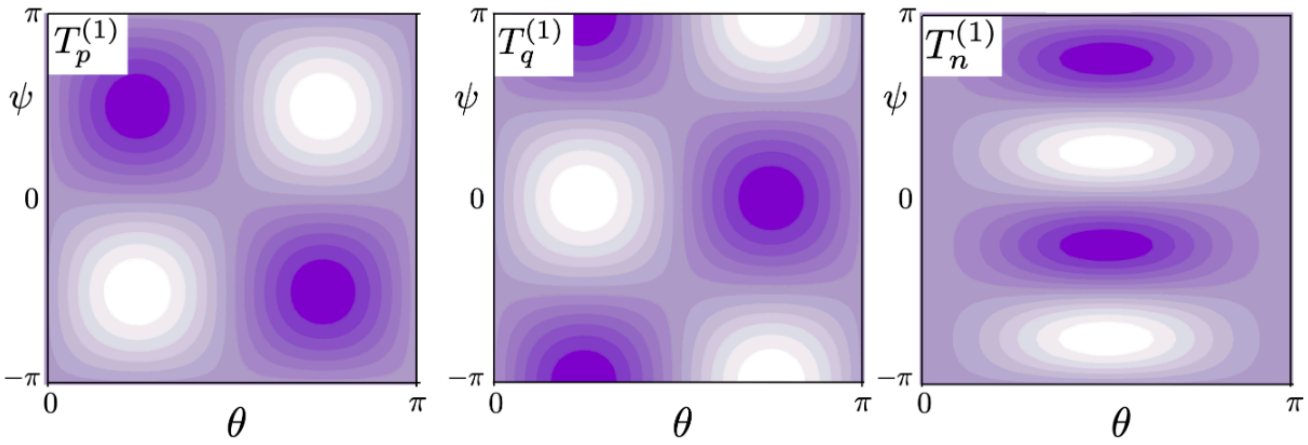

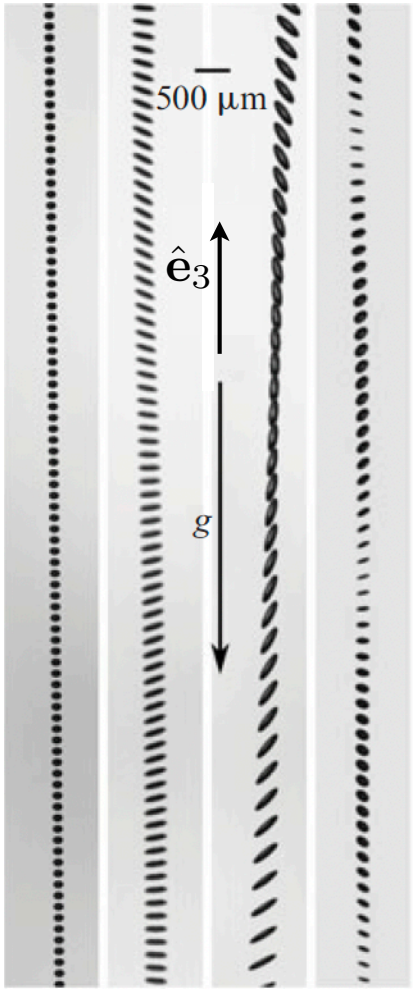

Ellipsoid

Sundberg, Candelier, Fintzi, Voth. Pierson, Gustavsson & Mehlig (2025)

Fluid-inertia torque on ellipsoid. From symmetry analysis:

$$T_p^{(1)} = 2N_{p(nq)}^{(vv)} v_n v_q + 2N_{p(nq)}^{(\omega\omega)} \omega_n \omega_q \,,$$
$$T_q^{(1)} = 2N_{q(pn)}^{(vv)} v_p v_n + 2N_{q(pn)}^{(\omega\omega)} \omega_p \omega_n \,,$$
$$T_n^{(1)} = 2N_{n(pq)}^{(vv)} v_p v_q + 2N_{n(pq)}^{(\omega\omega)} \omega_p \omega_q \,.$$

⇨ three parameters for $\boldsymbol{\omega} = 0$ (instead of one for spheroid).

Linear stability analysis: stable orientation must satisfy

$$N_{p(qn)}^{(vv)} < 0\,, \quad N_{q(np)}^{(vv)} > 0\,.$$
$$N_{n(pq)}^{(vv)} < 0\,, \quad N_{p(qn)}^{(vv)} > 0 \text{ for } \boldsymbol{q} \parallel \boldsymbol{e}_3$$
$$N_{q(np)}^{(vv)} < 0\,, \quad N_{n(pq)}^{(vv)} > 0 \text{ for } \boldsymbol{p} \parallel \boldsymbol{e}_3$$

⇨ broadest side down stable for nearly spherical ellipsoid.
In other words, theory explains experiment.

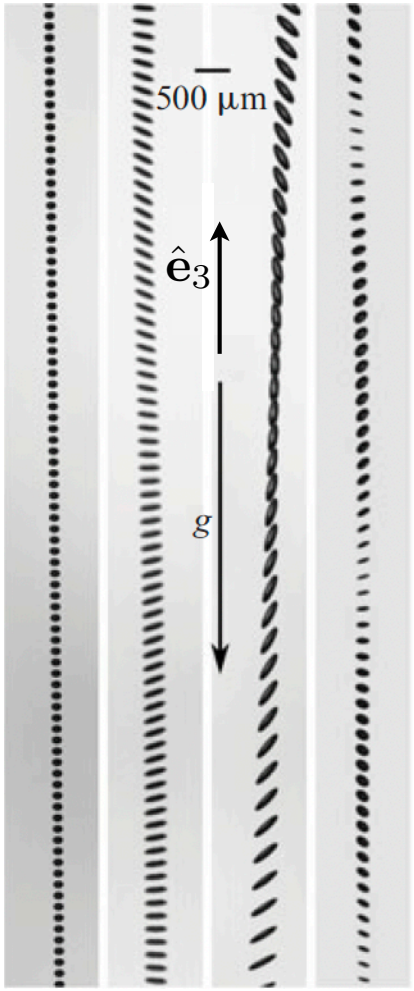

Helical ribbons

Huseby, Gissinger, Candelier, Pujara, Verhille, Mehlig & Voth, Phys. Rev. Fluids (2025)

Phase portrait of angular dynamics in Stokes limit

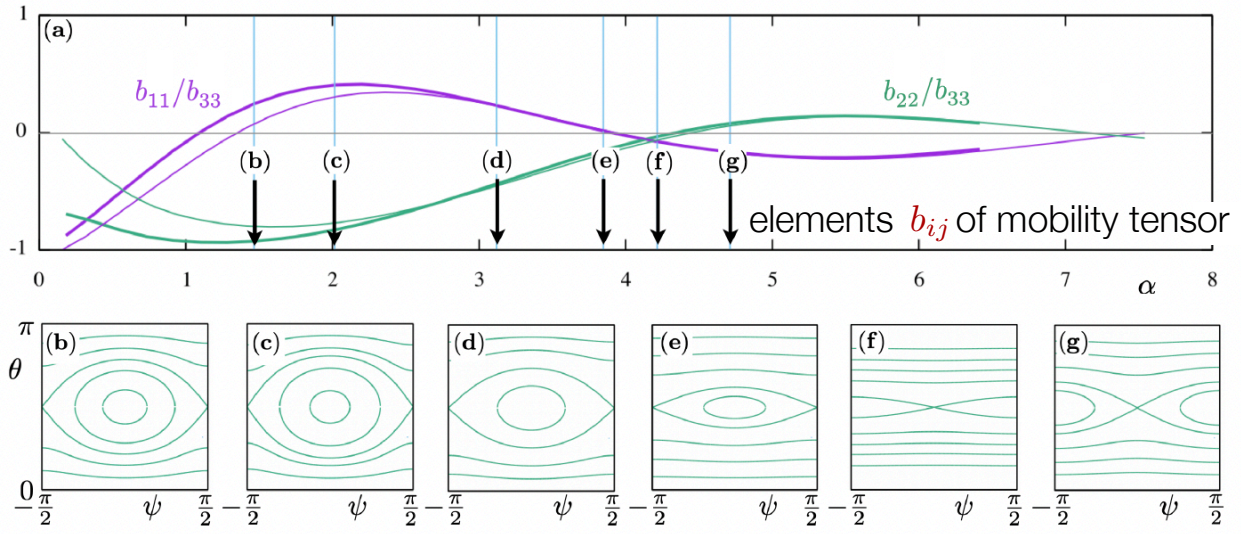

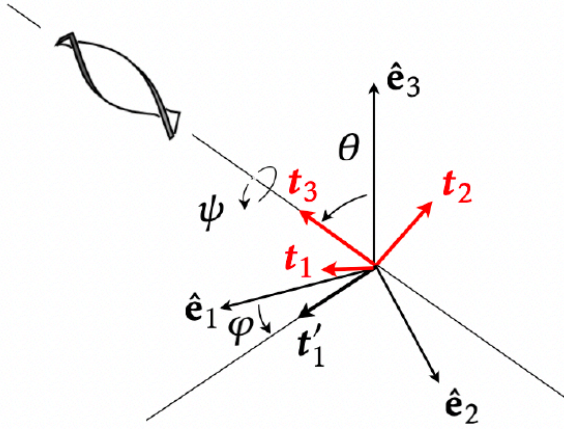

Shape and time-reversal symmetry ⇨ Hamiltonian phase portrait (constant of motion). Witten & Diamant, Rep. Prog. Phys. **83**, (2020) 116601

Time-reversal symmetry breaking (fluid inertia) turns tori into spirals. Resulting phase portraits remain to be worked out.

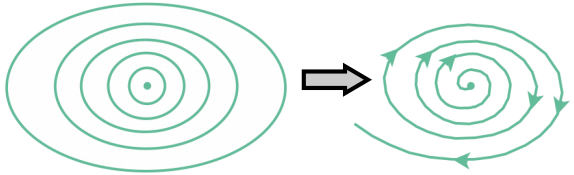

Point-group symmetry C_{2v}

Candelier *et al.*, Phys. Rev. Fluids (2025)

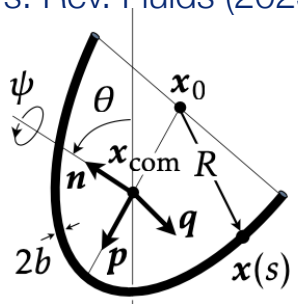

The particle shapes shown on the right both have C_{2v} symmetry
⇨ torques (including fluid-inertia contributions) parameterised in the same way:

$$\mathbb{B} = \begin{bmatrix} 0 & B_{pq} & 0 \\ B_{qp} & 0 & 0 \\ 0 & 0 & 0 \end{bmatrix}$$

$$\mathbb{N}^{(v\omega)}_{p::} = \begin{bmatrix} 0 & 0 & N^{(v\omega)}_{ppn} \\ 0 & 0 & 0 \\ N^{(v\omega)}_{pnp} & 0 & 0 \end{bmatrix} \quad \mathbb{N}^{(v\omega)}_{q::} = \begin{bmatrix} 0 & 0 & 0 \\ 0 & 0 & N^{(v\omega)}_{qqn} \\ 0 & N^{(v\omega)}_{qnq} & 0 \end{bmatrix} \quad \mathbb{N}^{(v\omega)}_{n::} = \begin{bmatrix} N^{(v\omega)}_{npp} & 0 & 0 \\ 0 & N^{(v\omega)}_{nqq} & 0 \\ 0 & 0 & N^{(v\omega)}_{nnn} \end{bmatrix}$$

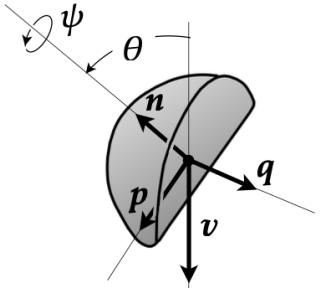

Miara *et al.*, Comm. Phys. (2024)

$\mathbb{N}$ - tensors have the same form as for ellipsoid.
Translation-rotation coupling due to non-zero $\mathbb{B}$.

These results explain steady torque on curved wires (previous slides).

Candelier, Gustavsson, Sharma, Sundberg,
Pumir, Bagheri & Mehlig, Phys. Rev. Fluids (2025)

History torque

History force on sphere decays slowly after sudden change of of particle dynamics, with BBO kernel $\sim t^{-1/2}$.

Landau & Lifshitz, *Fluid mechanics*, 2nd ed. (Pergamon Press, 1987)

History torque on sphere decays rapidly, kernel $\approx \delta(t)$.

Candelier, Mehaddi, Mehlig & Magnaudet, J. Fluid Mech. **954** (2023) A25

Consequence: no history terms in fluid-inertia corrections to Jeffery dynamics when $\mathbb{B} = 0$. Einarsson, Candelier, Lundell, Angilella & Mehlig, Phys. Fluids **27** (2015) 063301; Wang *et al*. (2025)

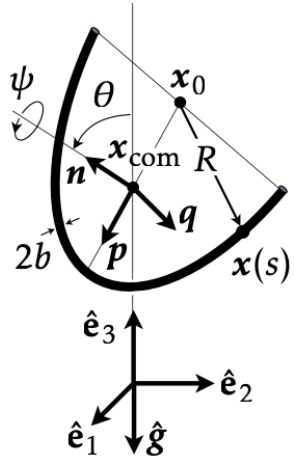

Here: when $\mathbb{B} \neq 0$, slowly decaying history torque

$$\boldsymbol{T}^{(1)}_{\rm sing} = \mathbb{B} \cdot \int_0^t \mathrm{d}\tau\, \mathbb{K}^{(1)}(t,\tau) \cdot \frac{\mathrm{d}\boldsymbol{f}^{(0)}(\tau)}{\mathrm{d}\tau} + \sqrt{\mathrm{Re}_p/\mathrm{Sl}} \int_0^t \mathrm{d}\tau\, \mathbb{K}^{(2)}(t,\tau) \cdot \boldsymbol{f}^{(0)}(\tau)$$

with $\boldsymbol{f}^{(0)} = \mathbb{A}\boldsymbol{v} + \mathbb{B}^{\mathsf{T}}\boldsymbol{\omega}$.

How the history torque changes the transient dynamics remains to be worked out for curved wires settling in quiescent fluid.

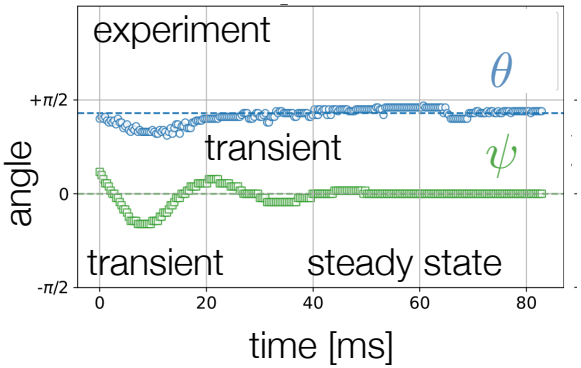

Isotropic helicoid

Lord Kelvin's isotropic helicoid

'An isotropic helicoid may be made by attaching projecting vanes to the surface of a globe in proper positions [...]. By making the globe and the vanes of light paper, a body is obtained rigid enough and light enough to illustrate by its motions through air the motions of an isotropic helicoid through an incompressible liquid' Lord Kelvin, "Hydrokinetic solutions and observations," Phil. Mag. **42**, 362 (1871)

Chiral octahedral symmetry implies $\mathbb{A} = A\mathbb{I}$, $\mathbb{B} = B\mathbb{I}$, $\mathbb{C} = C\mathbb{I}$, and $\mathbb{N}^{(v\omega)} = N^{(v\omega)}\boldsymbol{\epsilon}$ (with Levi-Civita tensor $\boldsymbol{\epsilon}$) ⇨ steady torque remains isotropic to order Re_p :

$$\boldsymbol{T}^{(1)} = -\frac{3v}{32\pi} B \left(\mathbb{I} - \tfrac{1}{3}\hat{\boldsymbol{v}} \otimes \hat{\boldsymbol{v}}\right) \cdot \left(A\boldsymbol{v} + B\boldsymbol{\omega}\right) + \underbrace{N^{(v\omega)}\, \boldsymbol{v} \wedge \boldsymbol{\omega}}$$

analogue of Rubinow-Keller lift force on rotating sphere

Rubinow & Keller, J. Fluid Mech. **11** (1961) 447

Epstein limit

Isotropic helicoid

Sarnitsky (2026)

Torque on isotropic helicoid in free molecular flow (Epstein limit: mean free path λ of gas $\gg$ particle size).

At small Mach number $\mathrm{Ma} = v/c_\mathrm{s}$, torque proportional to velocity, $\boldsymbol{T} = \mathbb{B}\boldsymbol{v}$.

Previous calculation yields zero translation-rotation coupling, $\mathbb{B} = 0$.
Dietler, Kusner, Kusner, Radon & Szymczak (2020)

Possible reason: calculation neglects shadows (previous results for translation-rotation coupling in free molecular flow for convex particles where shadows play no role). Livi, Di Staso, Clercx & Toschi, Phys. Rev. E **105** (2022) 015306

Calculation neglecting shadows (independent rods)

$$\boldsymbol{T} = 0 \quad \text{and} \quad \boldsymbol{F} \propto \left[8\boldsymbol{v} + \frac{1}{\sigma_v^2}\left(\tfrac{1663}{2888} v^2 \boldsymbol{v} + \tfrac{1079}{2888} \sum_{j=1}^{3} v_j^3 \hat{\mathbf{e}}_j\right) + \dots\right].$$

Numerical calculation with shadows: non-zero $\mathbb{B} = -10^{-4} \begin{bmatrix} 7.92 & -0.02 & -0.16 \\ -0.01 & 7.88 & 0.06 \\ 0.12 & 0.01 & 7.82 \end{bmatrix}$
(statistical error ± 0.15, one σ).

Aggregate particles

First stage of planet formation: collisions between small sand-grain aggregates in turbulent gas around growing star. Johansen & Lambrechts, Annu. Rev. Earth Planet. Sci. **45** (2017) 359

Mean free path $\lambda \sim 0.5\,\mathrm{m}$, aggregate size $a \sim 10\,\mu\mathrm{m}$.
Wilkinson, Mehlig, & Uski, ApJ Supplement Series **176 (**2008) 484

Essentially Epstein limit (Knudsen number $\mathrm{Kn} = \lambda/a = 5 \times 10^4$).

Little is known about drag force on porous (fractal) aggregates in the Epstein limit.

Recent laboratory experiments measure drag on porous aggregates of rods. Schneider & Wurm, AA **655** (2021) A50

Translation-rotation coupling? Angular dynamics expected to be important for outcome of aggregate collisions (sticking needed for planet formation).

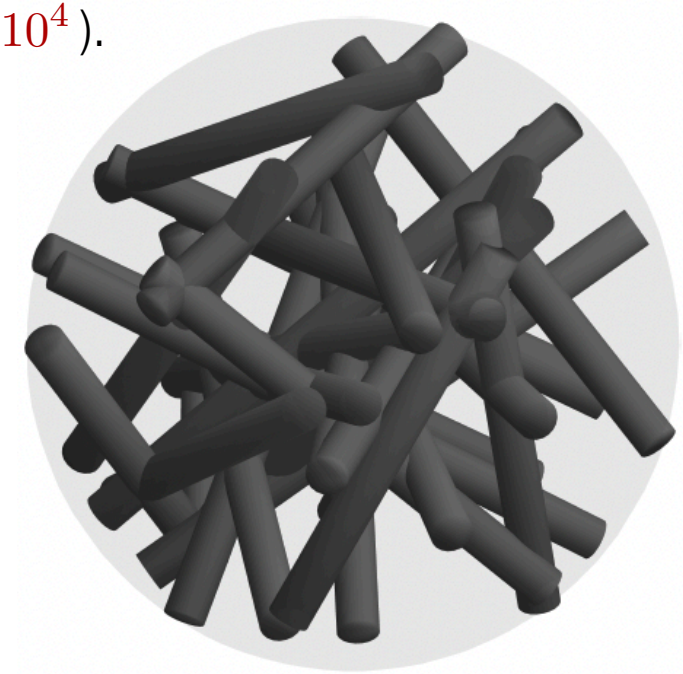

Schneider & Wurm, AA **655** (2021) A50

Conclusions

Angular dynamics of particles settling in quiescent (and turbulent flow) depends sensitively on shape, settling speed (Re_p), and particle Inertia.

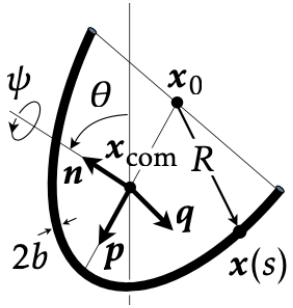

Angular dynamics of particles with increasingly asymmetric shapes: symmetry analysis allows to parameterise torques and thus the angular dynamics.

—Stokes limit and first-order Re_p-corrections

—Translation-rotation coupling $\mathbb{B}$ in quiescent fluid and shear flow

—steady and unsteady torques

—Epstein limit (free molecular flow) relevant for dust aggregates in accretion disks

Machine learning with neural networks

Cambridge University Press (2021)

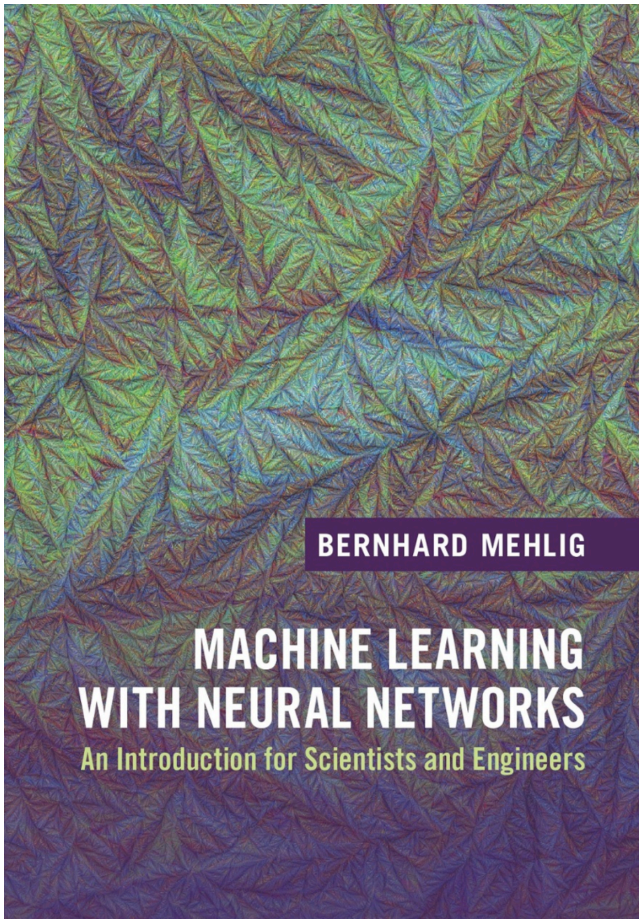

… Rather than presenting canned algorithms, this book tackles the fundamentals. As such, it is not for the faint hearted, but requires a sound background in theoretical physics …

Probert, *Contemporary Physics* (2022)